Advances in Geosciences Konstantinos Perakis & Athanasios Moysiadis, Editors
EARSeL, 2012

Material Reflectance Retrieval in Shadow Due to Urban Vegetation from 3D Lidar Data and Hyperspectral Airborne Imagery

Karine R.M. Adeline[1, 2], Xavier Briottet[1] and Nicolas Paparoditis[3]
[1]*ONERA, The French Aerospace Lab, 2 avenue Edouard Belin, BP 74025, 31055 Toulouse Cedex 4, France; Karine.Adeline@onera.fr, Xavier.Briottet@onera.fr*
[2]*Université de Toulouse, Institut Supérieur de l'Aéronautique et de l'Espace (ISAE), Toulouse 31055, France*
[3]*IGN – MATIS, 2 avenue Pasteur F 94165 Saint-Mandé Cedex, France; nicolas.paparoditis@ign.fr*

Abstract. Reflectance retrieval is a key parameter for land cover mapping from hyperspectral imagery. However most of the inverse methods to estimate these reflectances are limited in urban areas with the use of high spatial resolution sensors because they do not take into account the 3D radiative impact of the urban environment. A recent tool, ICARE [1], is able to retrieve surface reflectance in the reflective domain (0.4–2.5µm) in the sunlit and shadow areas overcoming both slope and environmental effects. Its main inputs are atmospheric conditions and the 3D vector model of the scene. This model has proven to perform with good accuracy in shadowed areas cast by opaque structures. Nevertheless ICARE has never been tested in the shadow of vegetation because the 3D information was not available. In this paper, a new dataset including 3D lidar (0.25m) and hyperspectral (CASI 0.5m) data acquired over Norrkoping is processed demonstrating the potential of ICARE to retrieve the surface reflectance over any type of shadows. The results will be assessed by comparing the retrieved reflectance of a given material both in the sunlit and shadow areas. Further, the gain brought by ICARE compared to a flat scene assumption reflectance retrieval method will be evaluated in terms of classification performances.

Keywords: Hyperspectral, 3D urban area, vegetation shadows, reflectance retrieval.

1. Introduction

The emergence of high spatial and spectral resolution for both airborne and spaceborne sensors from the visible to the short wave infrared domain (0.4-2.5µm), offers the possibility to extract more accurate material information from remote sensing imagery. For instance, some applications for land cover mapping require the knowledge of the spectral signature of materials. However, in urban environments, the strong spatial heterogeneity and the spectral variability of materials can make their identification and classification particularly complex [2]. Moreover, urban landscape often presents steep-sided relief like urban canyons. This strong 3D structure introduces a bias in the material retrieval from the at-sensor signal caused by environment and slope effects [3]. In this paper, the issue will only focus on ground material retrieval in shadows comparatively to sunlit areas in presence of urban relief.

Shadow detection and its correction have been largely studied over the last decades mainly with satellite and airborne data from medium to high spatial resolution. Recently, [4] gives a complete review of state-of-the-art shadow detection methods and further compares them each other over a large set of multispectral and hyperspectral airborne urban images acquired with a very high spatial resolution. Then, shadow restoration methods, also called "de-shadowing" methods, can be classed into three main categories: radiometric enhancement methods, 2D and 3D atmospheric correction methods. The first category aims to relight shaded areas with image-based techniques such as

histogram matching, linear-correlation correction, gamma correction, companion area mapping or invariant colour models [5, 6, 7, 8, 9]. Their major drawback is that they don't correct spectrally the signal from the atmosphere impact; which makes them very sensitive to sun and sky illumination. Then, the second and third categories overcome this problem by converting the at-sensor signal into reflectance through the use of a radiative transfer code. Nevertheless, 2D atmospheric correction is not adapted for shaded areas since they assume a flat field scene. Finally the last category accounting for 3D relief results to be the most appropriate to describe with accuracy the different interactions of light in a complex urban environment. Therefore, a recent 3D atmospheric correction tool ICARE [1] takes advantage of both a 2D atmospheric correction above the scene (with the help of 6S [10]) and a geometric computation with the knowledge of a 3D model of the scene.

From now, material reflectance retrieval has been successfully carried by ICARE over shadows cast by buildings with an absolute reflectance accuracy of at most 0.04 in comparison with ground truth spectral measurements. But, since ICARE only considers opaque reflective materials and no 3D tree model was available, its performances have never been tested over tree shadows which are partially transparent. Thanks to a new set of hyperspectral and 3D data, the aim of this paper is first to evaluate the gain brought by ICARE for material classification over any type of shadows. Then spectral signature of materials both in the sun and shade will be compared, especially for tree shadows in order to highlight the limitations of the correction of ICARE in the case of semi-transparent objects.

2. Methods

2.1. Atmospheric compensation

Before processing the data for remote sensing applications, the at-sensor images, expressed in radiance, are corrected from the atmosphere to retrieve the on ground reflectance. Two atmospheric compensation methods will be compared in both sunlit and shade.

Firstly, 6S is currently one of the most used 2D radiative transfer code with MODTRAN [11] for atmospheric correction problems. Nevertheless, its main limitation is it only considers flat field scenes. Secondly, ICARE is an inverse method model aiming at retrieving the ground reflectance from a radiance image and a 3D vector model of the scene by using some 6S atmospheric outputs and a radiative transfer code coupled to a geometrical 3D computation.

The equations used by 6S and ICARE are given in Table 1 with the considered modeled radiative terms illustrated in Figure 1. On the one hand, 6S cannot correct in shadows whereas on the other hand, ICARE assumes that the only difference between the shaded reflectance retrieval and its sunlit counterpart is the absence of direct sunlight.

2.2. Land cover classification and spectral signature of urban materials

Land cover classification performances on both the two atmospherically corrected at-sensor images from 6S and ICARE will be assessed through unsupervised K-means classification which results will be compared to manually built reference classification images. For that matter, two object clusters have been extracted on areas of interest over the at-sensor image: roads and vegetation. These two classes have been chosen as they represent the main part of typical urban landscape at ground. First, vegetation cluster has been deduced from the histogram thresholding of the vegetation spectral index NDVI [12] whereas roads have been delineated manually essentially near cast shadows. Then, the rest of the pixels will help to create a mask for the pixels not to classify.

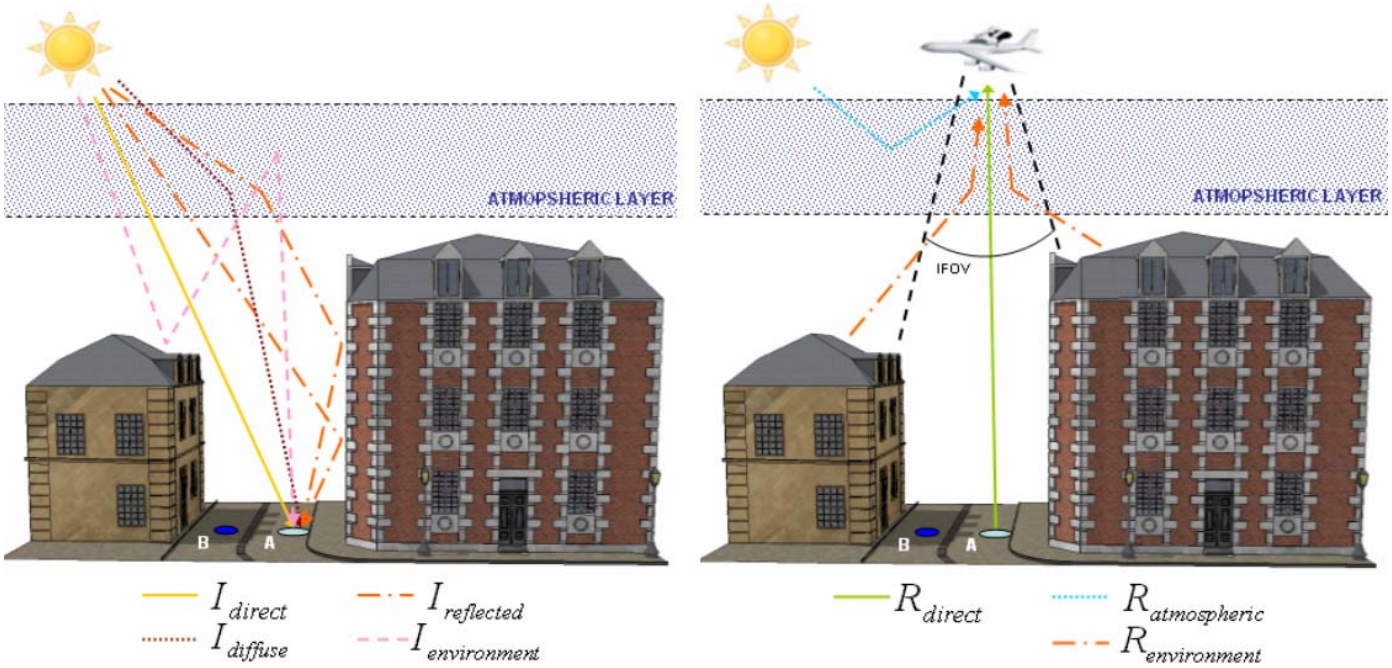

Figure 1: Radiative transfer modeling of ICARE and introduction of the different radiative components: irradiances (downward signals) and radiances (upward signals).

Table 1. Reflectance retrieval equations in the sun (target A) and shade (target B).

	6S	**ICARE**
Sun	$\rho_A = \frac{\pi(R_{sensor} - R_{atmospheric} - R^{2D}_{environment})}{T^{\uparrow}_{direct}(I^{2D}_{direct} + I^{2D}_{diffuse} + I^{2D}_{environment})}$	$\rho_A = \frac{\pi(R_{sensor} - R_{atmospheric} - R^{3D}_{environment})}{T^{\uparrow}_{direct}(I^{3D}_{direct} + I^{3D}_{diffuse} + I^{3D}_{reflected} + I^{3D}_{environment})}$
Shade	-	$\rho_B = \frac{\pi(R_{sensor} - R_{atmospheric} - R^{3D}_{environment})}{T^{\uparrow}_{direct}(I^{3D}_{diffuse} + I^{3D}_{reflected} + I^{3D}_{environment})}$

Where:

ρ : material ground reflectance in the sun or in the shade

I_{direct} : direct solar irradiance incident to the ground (3D: orientation of the target normal from the ground)

$I_{diffuse}$: downwelling irradiance scattered by the atmosphere (3D: sky viewing angle due to the 3D surrounding screening)

$I_{reflected}$: incident irradiance reflected at most twice in the 3D model of the scene (only for 3D modelling)

$I_{environment}$: irradiance due to multiple scatterings of light between the scene and the atmosphere (3D: sky viewing angle)

$T^{\uparrow}_{direct}$: atmospheric upward transmission computed by 6S

R_{sensor} : total at sensor radiance

$R_{atmospheric}$: upwelling radiance scattered by the atmosphere in the direction of the sensor

$R_{environment}$: upward radiance due to the scattered light from the surroundings and reaching the sensor

A shadow mask will also be built to evaluate the performances of the classification only over shaded areas for the two object clusters. It results from the spectral histogram thresholding method of [13]. Finally, the classification gain brought by ICARE over 6S atmospheric compensation will be compared in terms of good classification rate. Afterwards, the study will focus on the ICARE

reflectance retrieval for a given material in a tree shadow and for the same material in the sun. The calculation of a spectral similarity measure over the reflective domain (correlation coefficient) and the Root Mean Square Error (RMSE) will allow appreciating the accuracy of the material spectral signature retrieval in tree shadows.

3. Dataset and preprocessing

A set of airborne data acquired over Norrköping, Sweden, comprising of both hyperspectral and LIDAR data with very high spatial resolution, will allow us to show the benefit of using 3D information. An overview of the data characteristics are shown in Table 2. The collected image is composed of a mix of residential and commercial areas typical of a European urban landscape [14]. The largest object cluster present in the scene is vegetation mainly represented by aligned trees along roads, grass and private lawns. The percentage of shadows in the area is relatively important due to a solar inclination of 60.3° inducing long cast shadows by buildings and trees over a variety of materials such as roads and grass. For validation, three subsets are extracted from the principal image and the DSM, shown in Figure 2, and will be further studied. They have been selected because they contain both building and tree shadows which are easy to delineate for the making of the reference classification images.

Table 2. Dataset acquisition information.

Data	Acquisition date and time	Sensor characteristics	Spatial resolution
Hyperspectral image	September 2, 2010, 8:00-8:30 am	Push-broom sensor Itres CASI, 24 channels, 0.382-1.040µm, bandwidth 28.6nm	0.5m
Digital Surface Model (DSM)		LIDAR Optech ALTM Gemini	0.25m

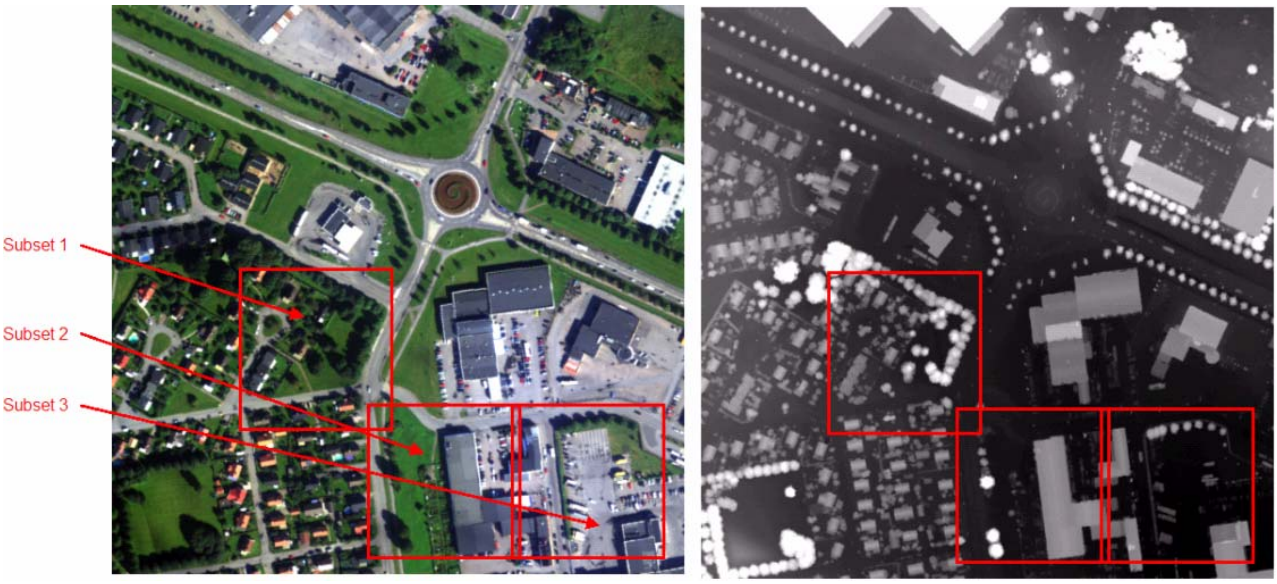

Figure 2: RGB composite image over Norrköping and selection of the subsets (left), DSM image in grey levels (right).

The hyperspectral image has to be calibrated. As no inlab calibration or ground truth measurements are available, a rough calibration is applied. It is based on the estimation of an absolute calibration coefficient at 550 nm supposing known the spectral reflectance of the lawn observed on the image and then using some white existing targets to achieve an interband

calibration in the other bands. The spectral reflectance of the short grass is taken from the database collected during the Capitoul trial [18]. Then, the atmosphere is chosen as a standard summer mid latitude profile and the aerosols a standard urban type with a visibility of 23km. Finally, a third processing step only selects the spectral bands which are ranged within the sensor sensitivity limit (0.44µm<lambda<1µm) and those whose atmospheric gaseous transmission is above 90% to limit the uncertainty we have on the atmosphere status. At the end, only 14 bands over 24 will be kept from 0.468µm to 0.869µm.

On the other hand, the subsets extracted from 3D data are smoothed with a Gaussian kernel filter in order to smooth the irregularities on the surface and to facilitate the triangulation operation of the 3D vector model necessary for the geometrical part execution of ICARE.

4. Results

4.1. Unsupervised classification K-means for land cover mapping issue

On the one hand, the results from K-means classification presented in Table 3 show that the classification results obtained with ICARE outperform those with 6S in the shaded areas. ICARE has around 75% of good performances in the shade by means over the three subsets and improves the overall classification of around 5% compared to 6S in both the sun and shade. Nonetheless, some errors are noticed on the borders of the shadow in the classified K-means images for ICARE presented in Figure 3. These bad classifications are due to the ground sampling accuracy of the LIDAR data coupled with misregistration problems between the LIDAR and the hyperspectral images.

Table 3. Overall good classification rates from Kmeans classification.

Subset 1	roads	vegetation	Total	
	sun and shade		sun and shade	Shade only (21.57% of total pixels)
6S	86.05%	67.04%	72.28%	18.84%
ICARE	95.63%	70.01%	77.06%	74.40%

Subset 2	roads	vegetation	Total	
	sun and shade		sun and shade	Shade only (11.24% of total pixels)
6S	78.91%	78.97%	78.94%	7.86%
ICARE	95.67%	72.21%	82.29%	76.71%

Subset 3	roads	vegetation	Total	
	sun and shade		sun and shade	Shade only (11.28% of total pixels)
6S	83.72%	69.80%	81.00%	7.17%
ICARE	93.08%	68.54%	88.28%	74.06%

Table 4. Good classification rates from Kmeans classification highlighting the performances of ICARE to correct in building and tree shadows over any type of material.

	Subset 1	Subset 2	Subset 3
building shadow	95.63%	95.67%	93.08%
tree shadow	70.01%	72.21%	68.54%

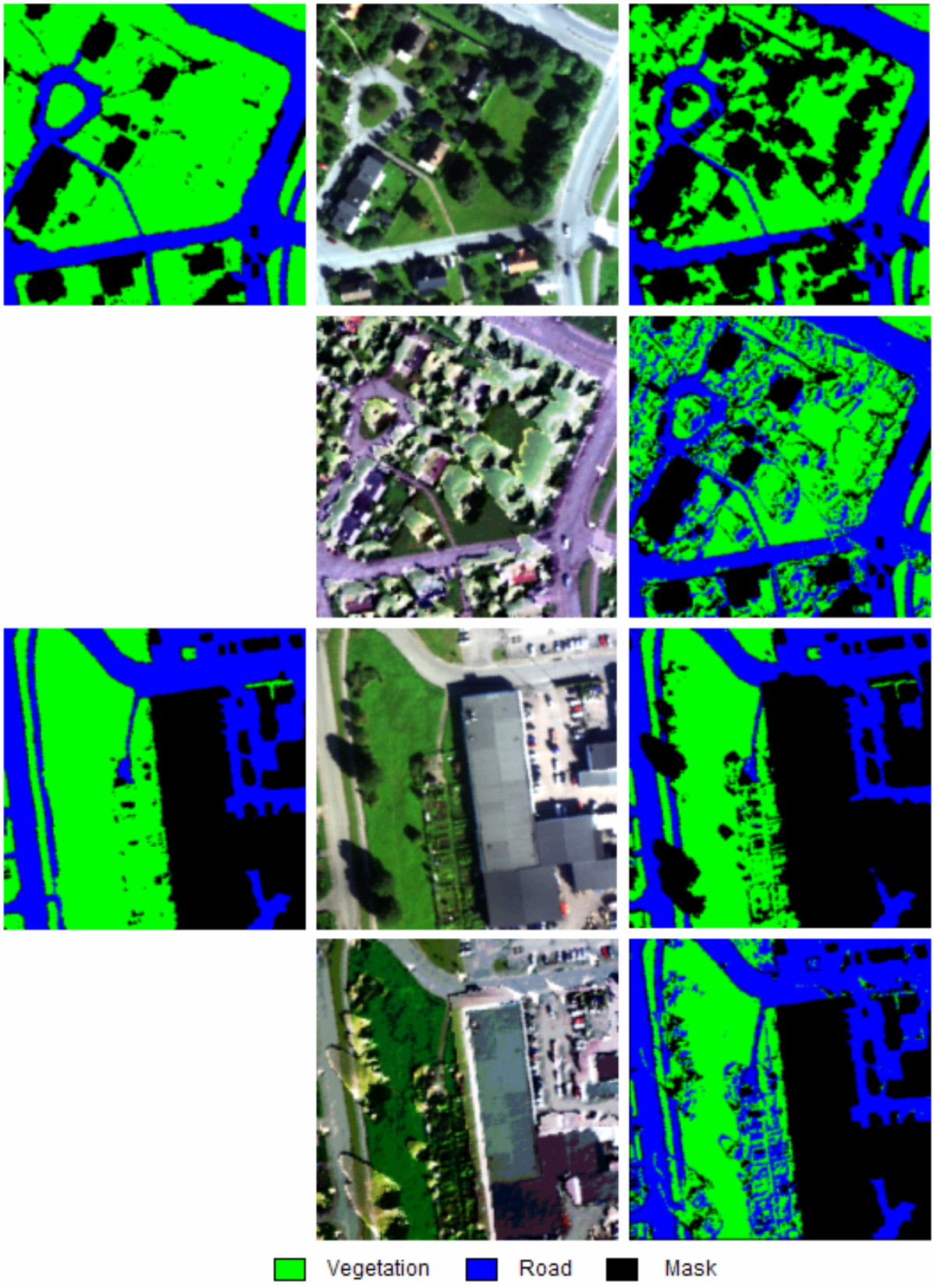

Figure 3: Results of the classification illustrated for subset 1 (top) and 2 (bottom): reference classification masks (first column), corrected reflectance images for 6S and ICARE (respectively second column, first and second row), classification images for 6S and ICARE (respectively third column, first and second row).

On the other hand, an analysis of the good classification rate in the shadow has been carried out with ICARE over building and tree shadows in Table 4. First results demonstrate that ICARE has better classification performances in building shadows (more than 90%) than in tree shadows (around 70%).

To conclude, 2D atmospheric compensation, like 6S, is appropriate for sunlit open areas but not for shaded areas since it neglects the radiative impact of the 3D geometric structure of the scene. Then, ICARE classifies with a good accuracy of above 90% in building shadows. This result was expected following previous studies using ICARE [1]. With the knowledge of the tree 3D model, K-means classification with ICARE is less accurate in tree shadows than in shadows cast by opaque 3D objects such as buildings. One reason is that trees are not fully opaque and a fraction of the downwelling irradiance is transmitted through the canopy. Since the total irradiance amount in the shadow is very low, this irradiance crossing the vegetation may have a non negligible impact.

4.2. Material spectral signature retrieval in tree shadows

Material reflectance retrieval comparison in the sun and shade will be conducted on three tree shadows over three types of material in subset 2 (Figure 4). Regions of interest are manually selected on the image in order to plot the mean and the standard deviation of the retrieved reflectances.

In Table 5, measures of spectral similarity with the correlation coefficient show that the spectral shape over the reflective domain is preserved in shade (R^2 above 98%), except for road where the spectrum is more distorted and less balanced between visible and near-infrared bands. RMSE values and a closer examination of the spectra plots in Figure 4 shows that the more we get closer from the tree location, the more the dispersion and band-to-band absolute error of reflectance values increase (RMSE from 1.50% to 8.81%). Actually, shadow is the darkest near the tree and the received signal at ground is the lowest. So the errors made close to the shadow borders (with neighbour sunlit areas) are accentuated close to the tree.

A second observation of the spectra plots points out that retrieved reflectances in the near-infrared bands have the highest standard deviation and errors compared to the visible bands before 697nm. Reflectance retrieval with ICARE effectively seems to be very noisy in this part of the reflective spectrum. One of the reasons can be the same as mentioned in section 4.1, that is to say ICARE reflectance retrieval in tree shadows is biased because it assumes no direct sunlight transmitted across the canopy at all. This light canopy transmission is more important in the near-infrared bands than the visible ones [16]. As such, an underestimation of the total irradiance received at ground causes an overestimation of the retrieved reflectance; which is noticeable on the plots for the near-infrared bands.

Finally, this study highlights the limitations of ICARE to retrieve material reflectance in shadows cast by non opaque 3D structure. More attention needs to be paid especially for near-infrared bands where the errors are the most important.

Table 5. Accuracy measures on the retrieved material spectrum in tree shadows compared to their sunlit counterparts in subset 2: correlation coefficient R^2 takes into account the reflectance means and RMSE estimates the standard deviation between the two spectra in terms of band-to-band reflectance difference.

Ground	Road			Grass			Bicycle path		
Location	Tree shadow (1)	Tree shadow (2)	Tree shadow (3)	Tree shadow (1)	Tree shadow (2)	Tree shadow (3)	Tree shadow (1)	Tree shadow (2)	Tree shadow (3)
Correlation coefficient (R^2)	8.78%	7.61%	7.73%	99.43%	99.60%	99.64%	98.46%	98.96%	99.30%
RMSE	3.17%	3.15%	3.16%	2.92%	1.50%	1.58%	8.81%	6.28%	4.74%

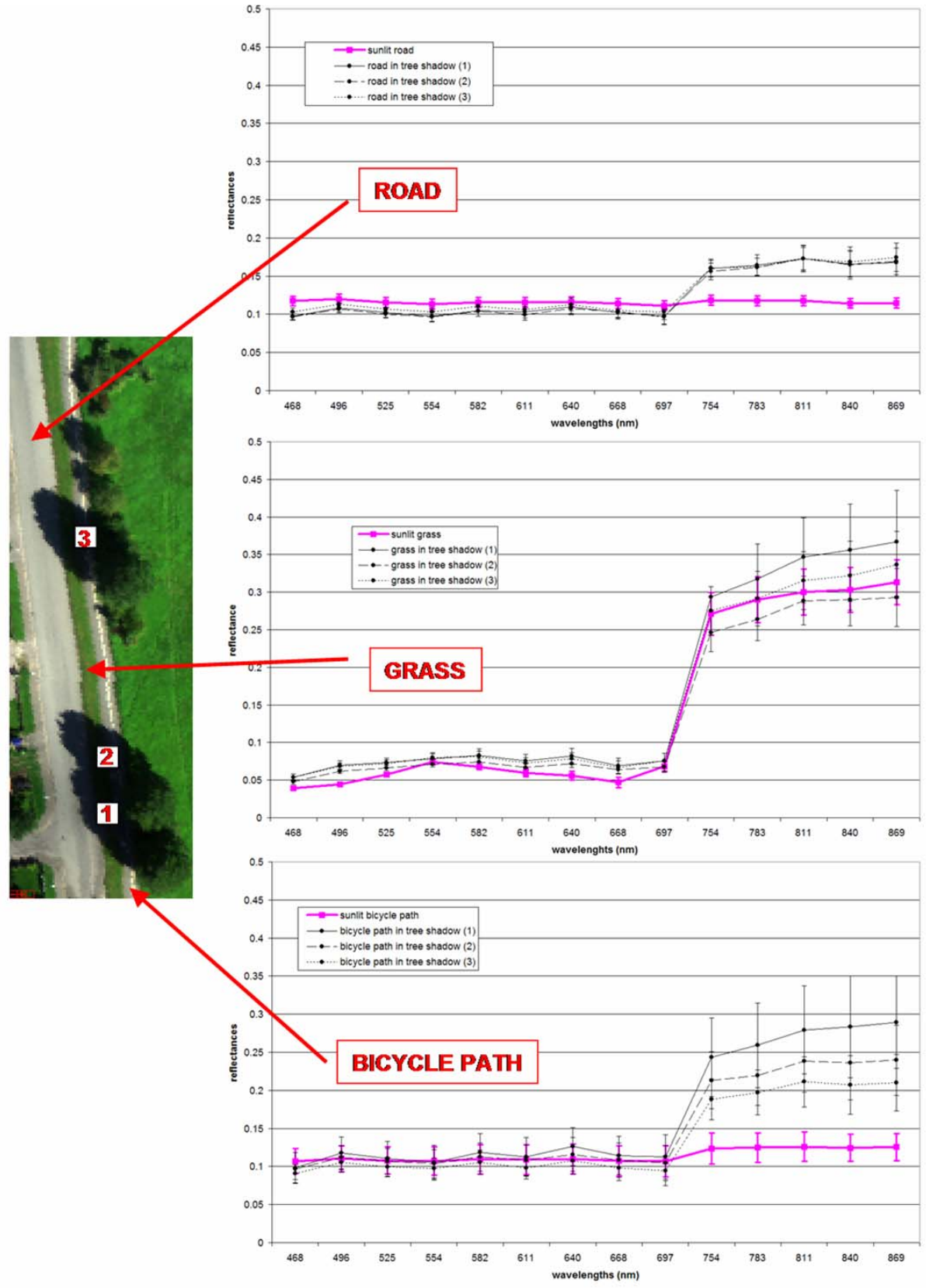

Figure 4: Selection of ROIs in three tree shadows over three ground materials for subset 2 (left side) and overlapping graphs of mean reflectance retrieval in the sun and shade for ICARE with standard deviation bar (right side).

5. Conclusions

The gain brought by using our 3D atmospheric compensation tool, ICARE, in regards with a 2D one, like 6S, is pointed out. This gain is about 5% for overall classification accuracy and it reaches from 56% to 69% for material classification in shadows. These improvements allow remote sensing applications such as land cover mapping, road extraction or urban change analysis to be more efficient in shaded areas for low sun elevation conditions. Nevertheless, the main limitations of ICARE, is that it considers all the materials of the scene as opaque 3D, which is not the case for tree. Moreover, it does not take into account the part of light transmitted through the canopy which can generate errors in the material reflectance retrieval with a RMSE of 9% at most for our three study cases, and strong distortion in near-infrared bands. Therefore, future works will include a sensitivity analysis in order to know the tree canopy parameters that have the most impact in the 3D radiative transfer modelling of ICARE. These parameters are of two kinds: spectral (reflectance and transmittance of the leaves, canopy and wood stems) and geometric (LAI, LAD), gaps in the canopy [17, 18]. Afterwards, ICARE will be adapted to tree shadows by considering not only opaque 3D materials, and new results will be compared to ground truth measurements.

Acknowledgements

We would like to thank Gustav Tolt from Sweden Defense Research Agency (FOI) for the Lidar 3D model and the hyperspectral image over Norrköping, and HPC-SA for providing the raytracer Raybooster (http://www.hpc-sa.com) implemented in the geometrical part of ICARE.

References

[1] Lachérade, S., Miesch, C., Boldo, D., Briottet, X., Valorge, C. and Le Men, H., 2008. ICARE: a physically-based model to correct atmospheric and geometric effects from high spatial and spectral remote sensing images over 3D urban areas. *Met. Atm. Phys.*, 102, pp. 209-222.

[2] Lacherade, S., Miesch, C., Briottet, X. and Le Men, H., 2005. Spectral variability and bidirectional reflectance behaviour of urban materials at a 20 cm spatial resolution in the visible and near-infrared wavelengths. A case study over Toulouse (France). *International Journal of Remote Sensing*, Vol. 26, No. 17, 10 September 2005, pp. 3859–3866.

[3] Miesch, C., Briottet, X. and Kerr, Y. H., 2004. Phenomenological analysis of simulated signals observed over shaded areas in an urban scene. *IEEE Transactions on Geoscience and Remote Sensing*, 42(2), pp. 434-442.

[4] Adeline, K. R. M, Chen, M., Briottet, X., Pang, S. K. and Paparoditis, N., submitted in 2012. Shadow detection in very high spatial resolution aerial images: a comparative study. *ISPRS Journal of Photogrammetry and Remote Sensing*, submitted status.

[5] Dare, 2005. Shadow Analysis in High-Resolution Satellite Imagery of urban Areas. *Photogrammetric Engineering & Remote Sensing*, vol.71, NO.2, February 2005, pp. 169-177.

[6] Chen, Y., Wen, D., Jing, L. and Shi, P., 2007. Shadow information recovery in urban areas from very high resolution satellite imagery. *International Journal of Remote Sensing*, Vol.28, NO.15, August 2007, pp. 3249-3254.

[7] Nakajima T., Tao, G. and Yasuoka, Y., 2002. Simulated recovery of information in shadow areas on IKONOS image by combining ALS data. *Proc. Asian Conference on Remote Sensing*. http://www.gisdevelopment.com/aars/acrs/2002/vhr/214.pdf

[8] Li, Y., Gong, P. and Sasagawa, T., 2005. Integrated shadow removal based on photogrammetry and image analysis. *International journal of remote sensing*, vol.26, NO.18, september 2005, pp. 3911-3929.

[9] Tsai, V. J. D., 2006. A comparative study on shadow compensation of color aerial images in invariant color models. *IEEE transactions on geoscience and remote sensing*, vol.44, NO.6, june 2006.

[10] Vermote, E., Tanré, D., Deuze, J. L., Herman, M. and Morcrette, J. J., 1996. Second simulation of the satellite signal in the solar spectrum: an overview. *IEEE Trans. Geosci. Remote Sens.*

[11] Berk, A. & al., 1999. MODTRAN4 radiative transfer modelling for atmospheric correction. *In: Proc. Optical Spectroscopic Techniques and Instrumentation for Atmospheric and Space Research III*, SPIE vol. 3756.

[12] Rouse, J. W., Haas, R. H., Schell, J. A. and Deering, D. W., 1973. Monitoring vegetation systems in the Great plains with ERTS. *in Proc. 3rd ERTS Symp.*, vol. 1, pp. 48–62.

[13] Nagao, M., Matsutyama, T. and Ikeda, Y., 1979. Region extraction and shape analysis in aerial photos. *Computer Graphics and Image Processing*, 10, pp. 195–223.

[14] Tolt, G., Shimoni, M. and Ahlberg J, 2011. A shadow detection method for remote sensing images using VHR hyperspectral and LIDAR data. *In proceeding of IGARSS*, 25-29 July 2011, Vancouver Canada.

[15] Masson, V., Gomes, L., Pigeon, G., Liousse, C., Pont, V., Lagouarde, J.-P., Voogt, J., Salmond, J., Oke, T., Legain, D., Garrouste, O., Lac, C., Connan, O., Briottet, X. and Lachérade, S., 2008. The Canopy and Aerosol Particles Interactions in TOulouse Urban Layer (CAPITOUL) experiment. Volume 102, Numbers 3-4 / December, 2008, *Special Issue on CAPITOUL Experiment (Special Editors: L. Gimeno, V. Masson and A. J. Arnfield), Meteorology and Atmospheric Physics*, Publisher Springer Wien, pp. 131-323.

[16] Jacquemoud, S., 2004. *Leaf optical properties. Reflection Properties of Vegetation and Soil, with a BRDF Data base* (M. von Shönermark, B. Geiger & H.P. Röser, Eds), Wissenshaft & Technik Verlag (Berlin), 352 pp.

[17] Asner, G. P., 1998. Biophysical and biochemical sources of variability in canopy reflectance. *Remote Sensing of Environement* 64, 1998, pp. 234-253.

[18] Widlowski, J-L., Verstraete, M. M., Pinty, B. and Gobron, N., 2003. *Allometric relationships of selected European tree species*. EC Joint Research Centre, Technical Report EUR 20855 EN, Ispra, Italy.